Tribology Letters, Vol. 18, No. 3, March 2005 (© 2005)
DOI: 10.1007/s11249-004-2752-9

Spatially resolved nanoscale chemical and mechanical characterization of ZDDP antiwear films on aluminum–silicon alloys under cylinder/bore wear conditions

M.A. Nicholls[a], P.R. Norton[a,*], G.M. Bancroft[a], M. Kasrai[a], G. De Stasio[b] and L.M. Wiese[c]

[a]*Department of Chemistry, University of Western Ontario, London, Ontario, N6A 2B7, Canada*
[b]*Department of Physics, University of Wisconsin-Madison, Madison, WI 53706-1390, USA*
[c]*Synchrotron Radiation Center, University of Wisconsin-Madison, Stoughton, WI 53589, USA*

Received 8 June 2004; accepted 3 October 2004

Understanding the lubrication of aluminum–silicon (Al–Si) alloys (>18% Si) under conditions similar to those in the cylinder/bore system is vital to determining their applicability to current engine designs. A novel investigation of the location of zinc-dialkyl-dithiophosphate (ZDDPs) antiwear (AW) film formation on an Al–Si alloy has been performed using X-ray absorption near edge structure (XANES) analysis, X-ray photoelectron emission spectroscopy (X-PEEM), and imaging nanoindentation techniques. A study of the initial stages of wear (10 min) to prolonged rubbing (60 min) was performed. The findings show that the film forms primarily on the raised silicon grains and is consistent with a zinc polyphosphate glass. The film has an elastic modulus of ~70 GPa and a similar elastic response to a ZDDP AW film formed on steel under the same conditions. This provides the first direct observation and characterization of a ZDDP antiwear film on Al–Si alloys using spatially resolved chemical and mechanical techniques at the nanoscale.

KEY WORDS: XANES spectroscopy, zinc dialky-dithiophosphate, aluminum alloy, silicon, wear, X-ray spectromicroscopy, mechanical properties, nanoindentation, phosphorus

1. Introduction

Aluminum–silicon alloys, with high silicon contents (>18%), are currently being investigated as cost effective replacements for cast iron components in internal combustion engines. One of the primary advantages of Al–Si alloys is the significant weight saving compared to that of cast iron components. Other advantages include low density, high strength-to-weight ratio, high thermal conductivity and low cost. The introduction of silicon improves the wear resistance of aluminium, and reduces the susceptibility to scuffing. Silicon forms separate hard phase grains in the aluminum matrix, thus providing better wear resistance. The primary location of Al–Si alloys is in the engine blocks, with the low Al–Si alloys being used in combination with sleeves or cast iron liners inserted in the bores. Cast iron liners are most widely used with an aluminum 6061 alloy engine block. The first aluminum cylinder block without liners was the Chevrolet Vega 2300 engine, produced by General Motors in 1970 [1,2]. This engine was a die cast hyper-eutectic aluminum-silicon alloy 390 (16–18% Si) in which the walls of the cylinder bores were electrochemically etched to expose primary silicon particles on the surface [1–3]. Other technologies currently being investigated include iron coatings [4–6] thermally sprayed on the aluminum bore walls. The trends and demands on the automobile manufacturing industry indicate the need to return to such weight saving technology. For example, Daimler-Benz now has many thousand Mercedes V-engines in the field with a hyper-eutectic Al–Si (23–26% Si) alloy engine block. The alloy used for the cylinder bores is a spray-compacted material produced by the Osprey process [7].

Thorough testing and investigation of the wear mechanisms of such materials needs to be explored. Not only are the wear mechanisms important to the understanding of engine failure, but also relevant to how these materials are lubricated. One of the primary antiwear and antioxidant additives in fully-formulated engine oils is zinc dialkyl-dithiophosphates (ZDDP). ZDDPs break-down under high temperatures and loads to form a sacrificial film at the contacting points in an engine. The sacrificial film has been observed using a direct observation wear machine (DOWM) [8,9] to form and wear away under the contact zone. The film has been studied using a multitude of surface analytical techniques [10–18] and it is well known that

*To whom correspondence should be addressed.
E-mail: pnorton@uwo.ca

the film formed is composed of a glassy polyphosphate structure [15,16,19–22]. Studies using X-ray absorption near edge structure (XANES) spectroscopy has shown that the film has a bilayer structure with short-chain zinc polyphosphates in the bulk (steel–substrate interface) and longer-chain zinc polyphosphates at the surface [16,22].

Scanning probe microscopy is also playing a crucial role in nanotechnology and surface characterization, and hence the topography and morphology of the ZDDP antiwear film has been examined using atomic force microscopy [6,22–29]. The surface has been found to be composed of regions of high elevation (termed "islands") and areas of lower lying regions ("valleys"). The island regions have also been termed antiwear pads. It has been suggested that the size and height of the antiwear pads are responsible for minimizing asperity contact between the rubbing surfaces and thus are responsible for reducing wear [25].

ZDDP antiwear pads have also been thoroughly studied by nanoindentation techniques [6,22,24–29]. The large pads have been found to have an indentation modulus ($E_s/(1-\nu^2_s)$) between 70 and 150 GPa. The pads have a convex shape. The center of the pads are responsible for bearing a larger portion of the load (compared to the edges) and have been found to have a larger indentation modulus than the edges [6,25]. Smaller (in size and elevation) antiwear pads have been found to have a lower indentation modulus (~30–75 GPa) [25]. Areas located between the pads have also been investigated using nanoindentation and have a much lower indentation modulus of ~25–30 GPa [24,25].

Advances in the area of synchrotron spectromicroscopy have now allowed for the acquisition of chemical information on the sub-micron length scale [30–32]. X-ray spectromicroscopy has been used to investigate tribological process in hard disk drives [33] and of tribologically derived ZDDP antiwear films [34]. The first ever high-resolution, identification of chemical species on the same length-scale as nanoindentation measurements of a ZDDP antiwear film was recently performed [22,35]. X-ray photoelectron emission microscopy (X-PEEM) was performed on selected features in a ZDDP antiwear film. The same features were characterized with both techniques via use of a microscopic grid of indent marks that allowed for their relocation. The authors found that (i) at the surface of the large antiwear pads there are longer-chain zinc polyphosphates, and (ii) in the lower-lying regions, between the antiwear pads, there are shorter-chain polyphosphates. Evidence found in the P L-edge spectra also indicated that some unreacted ZDDP is found in the valley regions between the antiwear pads. It was found, in agreement with others [6,22,24–29], that the large antiwear pads have an indentation modulus of ~81 GPa. This value is associated with the observation of longer-chain polyphosphates at the surface of the large pads. Tonck *et al.* [36] found results contrary to these in that the valleys had a higher indentation modulus than the islands.

A long-standing question in research on the wear of Al–Si alloys is the function of the silicon particles. It is generally thought that the grains, after honing and etching of the surface, act like riders that bear the load of the conforming surfaces. Very little research has been performed on the lubrication of Al–Si alloys using ZDDP [36–40]. The findings already published contain conflicting conclusions. In three of the four studies, the addition of the ZDDP additive to base oil had little or no effect in preventing wear. In two studies the authors used XANES [39,40] analysis to examine the wear scars for the presence of phosphorous decomposition products of ZDDP. The authors found that the ZDDP tribofilms, which form on the Al-alloys surfaces, are essentially identical to those that form on steel. It was also found that higher amounts of silicon has a significant effect on the ability to form a polyphosphate film [40].

An investigation into the occurrence (or lack thereof), and location of ZDDP antiwear film formation under lubricated wear of a high-silicon content (~18%) Al–Si alloy would be beneficial to understanding the applicability of such an alloy at the cylinder/bore interface. The investigation of a film formed at low loads on steel is compared to that formed on aluminum 390 (A390). XANES spectroscopy was used to explore the chemistry of the ZDDP antiwear film and X-PEEM was used to spatially resolve the chemical species in the films. The creation of a pattern of micro-indents on the surface allowed the same features to be relocated with an imaging nanoindenter and their nanoscale mechanical response to be measured. This provides new insight into the wear processes on high silicon content Al–Si alloys at low loads.

2. Experimental

2.1. Sample preparation and film formation

The aluminum 390 (A390) material was cast in the GM Research and Development Foundry (Warren, MI) as $300 \times 150 \times 25$ mm^3 chill blocks and diced using a wire electrode discharge machine to create $12 \times 12 \times 3$ mm^3 samples. The samples were then cut to $10 \times 10 \times 3$ mm^3 in size. The composition range of A390 is ~4–5% Cu, 16–18% Si, with small percentages of Mg, Fe, Zn and Ti. The sample was polished with 0.3 μm alumina and finished with 0.05 μm silica suspension. The steel samples were manufactured from 52100 steel into square specimens $10 \times 10 \times 4$ mm^3. The composition of 52100 steel is ~1% C, 1.3–1.6% Cr, the remainder being primarily iron. The sample was polished with 3 μm diamond paste. The

reciprocating cylinders were manufactured from 52100 steel with 6 mm diameter and 6 mm length. The steel sample and pins were austenitized and quenched. Their hardness was >60 Rockwell C. The pins were used as is. The samples were then cleaned with Ultra Sunlight® dish washing detergent (JohnsonDiversey, USA), then in methanol, and then hexane in ultrasonic baths for a minimum of 15 min in each.

The ZDDP antiwear films were formed in a reciprocating Plint wear tester [41] under boundary lubrication conditions with a cylinder-on-flat test geometry establishing a line contact. The test conditions consisted of rubbing times of either 10 or 60 min at 60°C, with a frequency of 25 Hz, load of 60 N and a 7 mm stroke length. The Hertzian contact pressure for such a geometry is ~0.264 and ~0.242 GPa for the steel and A390 surfaces respectively. A ZDDP commercial-concentrate was obtained from Imperial Oil, Canada. The concentrate is a mixture of neutral and basic forms, consisting of 85% secondary (C-4) and 15% primary (C-8) alkyls. The concentrate was diluted using MCT-10 base oil to 1.2 mass percent resulting in a phosphorus content of ~0.1% by weight. MCT-10 base oil is a mineral oil with a sulfur content of 0.12 mass percent and viscosity of 29.22 cSt at 40 °C and 5.05 cSt at 100 °C. A grid composed of indent marks was created using a Vickers hardness tester using loads of 25 and 200 g which made indents ~25 and ~150 μm across respectively. This grid allowed for relocation of the same regions with the multiple techniques discussed below.

2.2. Nanomechanical property testing

Details of the instrumentation and set-up are given elsewhere [6,22]. A hybrid indenter, with a Hysitron force transducer® and an AFM scanner, was used to image the surface of a sample with a resolution of ~100 nm or better, and quantitatively measure the nanomechanical properties of the sample using the same tip. Perpendicular tip-sample contact was maintained using a Digital Instruments "JV" vertical engage scanner. The indenter tip is a three-sided Berkovich diamond with an elastic modulus $E = 1140$ GPa and Poisson's ratio $\nu = 0.07$. The average tip radius of a Berkovich diamond is between 100–160 nm. Topographic images were taken before and after each indent. This allowed for selection of a region that was smooth and free of any height abnormalities that would affect the contact geometry and hence the contact mechanics. The elastic modulus is determined using the Oliver–Pharr method [42]. This method is based on the assumption that the elastic modulus is independent of indentation depth. The reduced modulus is defined through the equation $1/E^* = \{[(1-\nu^2_s)/E_s] + [(1-\nu^2_i)/E_i]\}$ where E_s and ν_s are the Young's modulus and Poisson's ratio of the sample and E_i and ν_i are the respective values for the indenter. The system was calibrated for compliance and tip abnormalities, using the commonly accepted method of measuring a succession of indents into fused silica at different penetration depths to calculate the tip area function [43–45]. This value is used in the calculation of the reduced modulus, E^* of the tip–sample interaction. If the Poisson's ratio of the material being tested is known (ν_s), the corrected modulus, E_s for the sample can be calculated using E^*, E_i, ν_s and ν_i in the above equation. The values listed in this report are the indentation modulus of the sample E_s^*, given by $E_s^* = E_s/(1-\nu^2_s)$ in which the tip properties have been removed from the reduced modulus value. Indents were taken into the film to maximum loads of 25 μN, unless otherwise stated. This minimized the influence of the lower-lying substrate and kept the penetration into the film to ~10% [43,46,47]. Several alternative approaches to the calculation of elastic moduli for thin films on rigid substrates have been devised [46–53]. In an attempt to fully understand the mechanical response of the ZDDP films, we previously employed [22] the method of Song and Pharr [52]. Simply, the indentation modulus of the film can be separated from that of the steel using the following equations [52]:

$$\frac{1}{E_s^*} = (1 - I_0)\frac{1}{E_{steel}} + I_0\frac{1}{E_f}, \tag{1}$$

where

$$I_0 = \frac{2}{\pi}\arctan\left(\frac{t}{a}\right) + \frac{1}{2\pi(1-\nu)}\left[(1-2\nu)\frac{t}{a}\ln\frac{1+\left(\frac{t}{a}\right)^2}{\left(\frac{t}{a}\right)^2} - \frac{\left(\frac{t}{a}\right)}{1+\left(\frac{t}{a}\right)^2}\right] \tag{2}$$

and E_s^* = the indentation modulus of the sample (film + steel; defined above), E_f is the modulus of the film, $E_{steel} = 240$ GPa, $E_{Si} = 174$ GPa (determined below), t = the film thickness, and assuming the Poisson's ratio for steel, silicon and the film are the same $\nu_{steel} = \nu_{Si} = \nu_f = \nu = 0.3$.

2.3. Surface imaging and roughness measurement

Topographical imaging was performed using a Digital Instruments Nanoscope IIIa® atomic force microscope. Images were obtained in constant-force mode to investigate the morphology and topography of the blank substrates, wear scars and antiwear films after formation. Topography images were taken at 10 different locations on the surface. The 100×100 μm^2 images were then processed using Digital Instruments® software to determine the average surface roughness

(R_a) of each sample. A LEO-440 scanning electron microscope with a Quartz Xone Gresham light element detector was used to image the surfaces in field-emission and backscattering modes and perform X-ray analysis.

2.4. XANES and X-PEEM analysis

X-ray absorption spectra provide detailed information about the local environment and oxidation state of elements in a film or on a surface. XANES analysis employs the use of soft X-rays making it a non-destructive technique. XANES spectroscopy was performed at the Canadian Synchrotron Radiation Facility at the 1 GeV Aladdin storage ring, University of Wisconsin, Madison. The L-edge data were obtained using the Grasshopper beamline which has a resolution of ~0.1 eV at the P L-edge. The K-edge data were recorded using the double crystal monochromator (DCM) beamline with a photon resolution of ~0.9 eV. Spectra were recorded using the total electron yield (TEY) and fluorescence yield (FY) detection modes, details of which can be found elsewhere [54]. At least two individual scans were recorded for each specimen and digitally combined. The spectra were normalized against I_o and a linear background was subtracted.

X-ray photoelectron emission microscopy was performed using the SPHINX [55] microscope (ELMITEC GmbH) installed on the 6m-TGM (Toroidal Grating Monochromator) beamline at the 1 GeV Aladdin storage ring, University of Wisconsin, Madison optimized to give ~0.1 eV resolution at the P L-edge (for details see references [22,35,56]). Image intensity in X-PEEM is proportional to the TEY and the surface sensitivity was limited by the escape depth of the secondary electrons at the P L-edge (3–5 nm) [56,57]. Spectromicroscopy images were taken with 0.1–0.2 eV step sizes. A 100 μm field of view was chosen for the selected area with a resolution of ~200 nm per pixel. The images were combined to produce a three-dimensional data set or spectromicroscopy "stack" [30] that was analyzed to extract detailed chemical information about the tribofilm using aXis2000 software [58,59]. The software allows for selection of a single pixel, or regions of several pixels in size to extract XANES spectra. The spectra resulting from the selected regions are an average spectrum over all the pixels contained in the region. Thus some spectra are the average of a few pixels (usually have poor signal-to-noise) or several tens to hundreds of pixels. Images were dominated by other contributions to the signal generation process—topography, shadowing, charging, variable sampling depth and work function, among others. Thus one of the challenges of this work was to develop and use analysis techniques that emphasized the chemical (X-ray absorption) information while simultaneously de-emphasizing the other contrast factors. Many regions were selected for spectra extraction; regions that had interesting features such as high or low signal intensity, were in and around silicon particles, or were large or small antiwear pads. Spectra were chosen from areas that had decent signal to noise ratios. Stacks were acquired at the phosphorus L-edge (130–160 eV) and analyzed for differences in chemistry. Unfortunately, stacks acquired at the sulfur (155–190 eV), silicon (120–195 eV), and aluminum (65–90 eV) L-edges generally did not detect significant amounts of each element to discern changes.

3. Results and discussion

3.1. Analysis of blank 52100 steel and A390 samples

The roughness of the polished surfaces was measured using AFM (see experimental). The average roughness (R_a) for the 52100 steel and A390 samples were measured to be 6.0 ± 0.6 and 68 ± 11 nm respectively. The larger roughness for the A390 sample is due to the silicon grains protruding from the surface after the polishing process. Other features included, pits formed due to gases that were introduced during the casting of the alloy. A SEM image of the polished A390 surface is shown in figure 1(a). Alloying inclusions can be observed throughout the aluminum matrix. Differences in contrast, in the backscattered SEM image, are due to the different atomic numbers of the alloying elements. Figures 1(b)–(e) show the EDX maps of the major constituents in the alloy. A clear contrast between the aluminum matrix and silicon grains can be identified. Inclusions of copper and iron can also be found along with detectable amounts of magnesium and manganese. AFM imaging, and cross-sectional analysis, of the polished A390 surface, showed that on average the silicon grains protruded from the surface by 30–100 nm.

Nanoindentation measurements were made on the polished 52100 steel and A390 surfaces. Topography images were taken before and after each indent with the same tip. Force–distance (f–d) curves were taken to loads varying between 50 and 300 μN. Representative f–d curves for 300 and 50 μN are shown in figure 2(a) and (b), respectively. Due to the capabilities of the imaging nanoindenter, f–d curves were taken on the aluminum matrix and separately on the silicon grains. The indentation moduli (E_s*) were calculated from between 16 and 21 curves taken on the steel, aluminum matrix, and silicon grains using the technique suggested by Oliver and Pharr [42] which utilizes the initial slope of the unloading curve. The E_s* values,

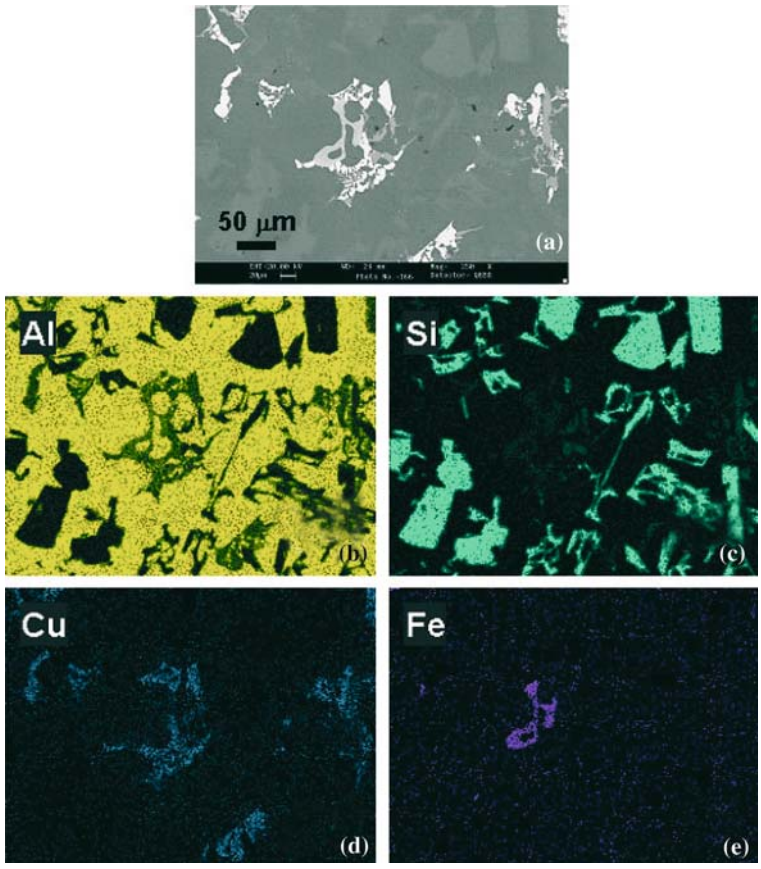

Figure 1. A backscattered SEM image is shown in (a) for blank, polished A390. The corresponding EDX elemental maps are shown for aluminum (b), silicon (c), copper (d) and iron (e). The bright contrast in images (b)–(e) indicates a high abundance of the particular element.

calculated from *f–d* curves, were averaged together to determine the final value. The statistical errors given for these averages represent a standard deviation of 2σ. The E_s* values for steel, aluminum matrix, and silicon grain are 253 ± 15, 129 ± 15 and 174 ± 18 GPa.

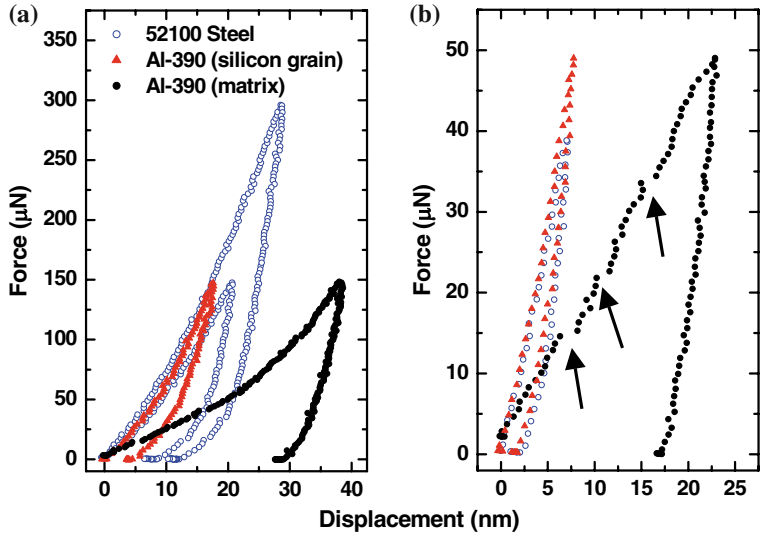

Figure 2. Force–distance (*f–d*) curves are shown for the blank, polished substrates. *f–d* curves taken to large maximum loads are shown in (a) and to lower loads in (b). The ability of the imaging nanoindenter allows for measurement of both the Al-matrix and the silicon grains. Dislocations can be observed in applied-load portion of the *f–d* curve taken into the Al-matrix. These dislocations are due to the fracturing of aluminum oxide (arrows).

f–d curves taken in the aluminum matrix also detected the effect of the aluminum oxide present on the surface. Low load (50 μN) *f–d* curves are also shown in figure 2(b). Dislocation movements can be detected in the *f–d* curves (identified by arrows) that are due to the abrupt tip movement after the oxide fractures. Typical oxide thickness found on aluminum is on the order of 2–5 nm [60]. The first dislocation in the *f–d* curve taken on the Al-matrix corresponds to this very closely. The slight difference could be due to a thicker oxide formed from the mechanical polishing, or due to roughness of the Al-matrix. Comparison of the *f–d* curves taken to this load (50 μN), for the steel and silicon grains, shows that they have a very similar elastic response. This contrasts significantly with the data for the aluminum matrix which exhibit a much larger hysteresis due to the large plastic deformation of the surface as the tip is forced into the matrix.

3.2. Macro XANES analysis, initial stages of wear

Antiwear films were formed in a ZDDP solution for 10 min rubbing-time, 60 N, 25 Hz at 60 °C for 10 min rubbing, were investigated to spatially resolve any film formation on either 52100 steel or A390 surface.

L-edge spectroscopy probes the excitation of electrons from 2p occupied orbitals to unoccupied antibonding orbitals. Model compounds, with known composition, are used as reference materials to identify the Si species present in the film. The large area spectra are obtained from an X-ray spot size ($\sim 2 \times 3$ mm^2) and give an overall average spectrum for the antiwear film. It is well known that the TEY and FY measurements of the photoabsorption are proportional to the absorption coefficient. The differences between the TEY and FY modes of measurement are based upon the detection limit of each technique. The TEY mode is a surface sensitive technique probing 2–5 nm at the Si L-edge (120–160 eV) and FY mode is a bulk technique, probing <50 nm [57]. Figure 3(a) shows the TEY and FY measurements taken at the Si L-edge of a silicon wafer. Three main peaks labeled 1–3 can be observed in the Si L-edge TEY spectrum. Peak 1 (a doublet due to the spin–orbit coupling) is assigned to the transition of electrons from the Si 2p to 3s-like *a* orbitals [61,62]. Peak 2 is the corresponding doublet for SiO_2. Peak 3 has been assigned to the transition of Si 2p electrons to 3p-like t_2 states in SiO_2 [54,61,62]. The increased probing depth of the FY mode results in an almost oxide-free spectrum, for silicon. Peaks 2 and 3 (with much reduced intensities) can be observed. In the antiwear film (bottom spectrum), the TEY spectrum had a poor signal to noise ratio indicating that the surface is covered by the antiwear film, and is thus not shown. The FY spectrum (bottom) also shows a strong indication of oxidation after rubbing with no elemental silicon detected.

The K-edge spectra for the antiwear film along with those of model compounds are shown in figure 3(b). The sensitivity of the TEY and FY modes at the Si K-edge (1830–1900 eV) is 50 and >500 nm respectively [57]. The main peak in Si wafer is due to the Si 1s electrons being promoted to 3p-like t_2 states [62]. A strong white-line for silicon can be observed at ~1838.4 eV (peak 1). The spectrum taken of a silicon sample with 210 angstroms of an anodically grown oxide layer is

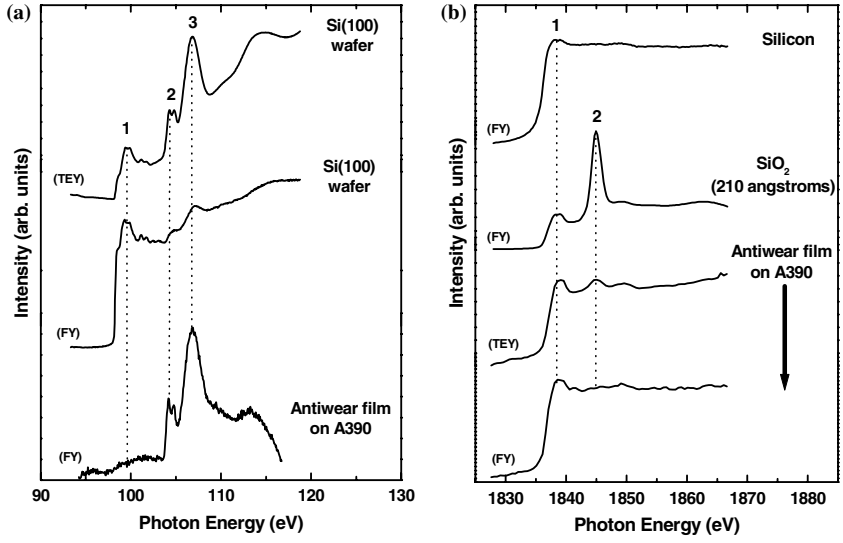

Figure 3. The silicon L- (a) and K-edge (b), XANES spectra of silicon, compared to the macro-scale spectra obtained from the antiwear film on A390 (10 min rubbing-time). Peak 1 is representative of silicon and peaks 2 and 3 for silicon oxide.

also shown. A strong peak 2 is due to the silicon oxide (SiO_2). These similar features can be observed in the TEY spectrum of antiwear film indicating that the oxide layer is very thin. The FY spectrum from the antiwear film shows primarily silicon.

The Al L-edge TEY and FY spectra (figure 4) of aluminum metaphosphate, $Al(PO_3)_3$, low-silicon Al-alloy sample A6061 (~0.7% Si), and the antiwear film on A390 sample are shown. Peak a (doublet) in the FY spectrum is due to the transition of electrons from the 2p to 3s-like *a* orbitals in metallic aluminum and peak b, in the TEY spectrum is the corresponding transition for aluminum oxide. Broad peak c, is due to the transition of electrons to 3p-like *t* orbitals of aluminum oxide species [63]. It can be observed that the TEY spectrum of the antiwear film shows the presence of both metallic aluminum and aluminum oxide species; whereas the FY spectrum show mostly metallic Al and a trace of aluminum oxide, in contrast to Si (figure 3(a), bottom). It can also be observed that no aluminum metaphosphate can be distinguished in the film. This is an indication that the Al oxide is present only on the surface and is mixed with antiwear film.

Phosphorus L- and K-edge spectroscopy provides detailed oxidation and local geometry information about the P species present in the ZDDP antiwear

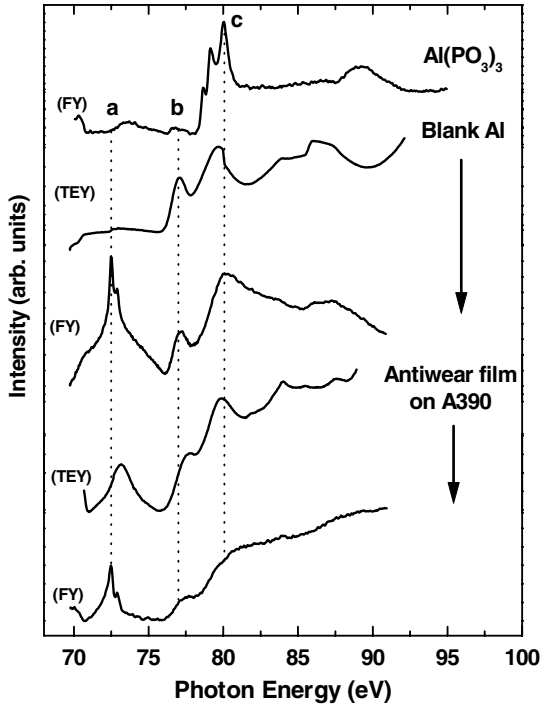

Figure 4. The aluminum L-edge, macro-scale XANES spectra of blank A6061 Al-alloy compared to the macro-scale spectra taken from the wear scar on the A390 sample (10 min rubbing-time). Peak *a* is due to aluminum, and peaks *b* and *c* are due to aluminum oxide. A significant amount of aluminum (peak *a*) can be detected in both at the surface (TEY) and in bulk (FY) spectra from the A390 wear scar. The TEY spectrum shows a strong aluminum oxide signal (peaks *b* and *c*).

films. The sampling depths of the TEY and FY at the P L-edge are 5 and 60 nm respectively [57]. The K-edge surface sensitivity is ~50 nm for the TEY mode and >800 nm in the FY mode [57].

In figure 5(a), the spectrum from the ZDDP antiwear film shows its characteristic triplet structure [16]. Considering the P L-edge spectra (figure 5(a)), peaks a, b, and c of the model zinc pyrophosphate are shifted to higher energy from peaks 1, 2, and 3 of unreacted ZDDP. Comparison of the standard ZDDP antiwear film formed on 52100 steel to the model zinc polyphosphate indicates that ZDDP has decomposed and formed a zinc polyphosphate on the surface. Spectra A and A′ (TEY and FY) obtained from a film generated using a 52100/52100 (coupon/pin) couple at the same temperature and frequency and concentration of ZDDP solution, however at 220 N load with 60 min. rubbing. Peaks *a* and *b* are the 2p spin–orbit doublet, separated by 0.8 eV. They are assigned to the transitions of electrons from occupied $2p_{3/2}$ and $2p_{1/2}$ levels to unoccupied anti-bonding orbitals. Peak *c* is attributed to the transition of the 2p electrons to a *p*-like t_2* molecular orbital. The ratio of the relative peak heights of either peaks *a*:*c* or peaks *b*:*c* provide a semi-quantitative indication of the number of P in the polyphosphate chain length; the larger the ratio, the longer the chain length [21,22,64]. It has previously been found that ZDDP antiwear films formed on steel, form a bilayer structure with long-chain polyphosphates at the surface and shorter-chain polyphosphates ($Zn_2P_2O_7$) found closer to the film/metal interface [16,22]. The TEY and FY spectra (A and A′) of the standard film (found to have good antiwear characteristics) are compared to spectra B and B′; C and C′ of those formed at the lower load and rubbing time formed on 52100 steel and A390, respectively [14,16]. It can be observed that the film formed on 52100 steel at the short rubbing time and lower loads is a shorter-chain polyphosphate film with the chain-length being essentially the same from the surface to the bulk of the film (insignificant difference in peak *a*:*c* ratios). Likewise at the lower load and shorter rubbing time, the film formed on the A390 sample is a shorter-chain polyphosphate. The FY spectrum (C′) of the A390 sample has a poor signal to noise ratio indicative of a thin film. It may also be concluded from comparing the TEY to the FY that the bulk of the film may actually be formed of a slightly shorter-chain length ortho- or pyrophosphate. Model zinc polyphosphates were compared to aluminum meta and polyphosphates (see below for an example), however no significant shifts or changes in near-edge structure were observed. Thus it cannot be concluded whether a zinc or aluminum phosphate is formed. It is most probable that a zinc phosphate film forms with some intermixing with aluminum cations near the film/metal interface.

The corresponding P K-edge results are consistent with those from the P L-edge. It can be observed in

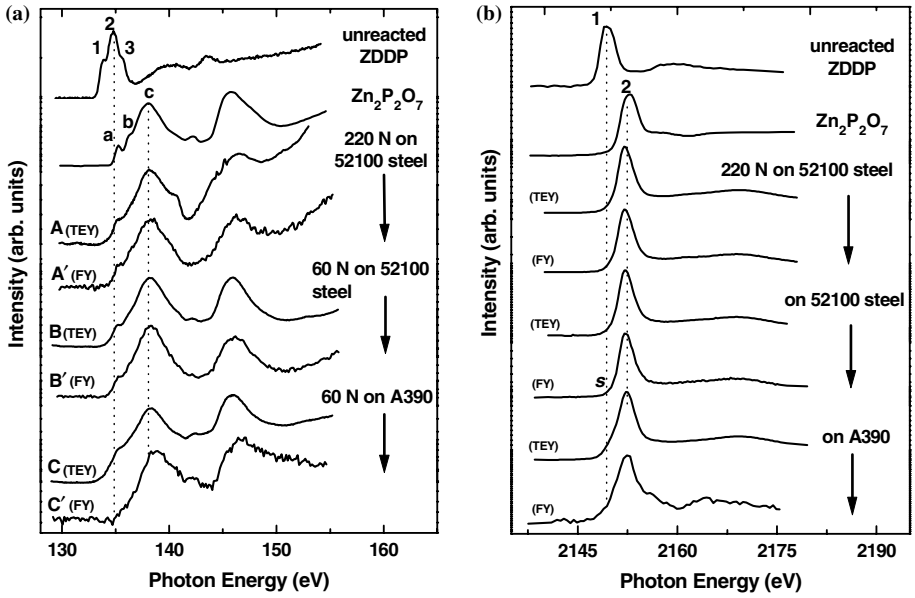

Figure 5. Phosphorus L-edge (a) and K-edge (b) macro-scale XANES spectra of unreacted ZDDP and a model polyphosphate ($Zn_2P_2O_7$) are compared to ZDDP antiwear films (10 min rubbing-time). Peak assignments can be found in the text. Spectra A and A′ are for a standard film formed under higher pressures (220 N), spectra B and B′ are for the film formed on 52100 steel (at 60 N) and spectra C and C′ on A390 (at 60 N). It can be observed that the surface (TEY) and bulk (FY) spectra show small differences in peak intensities of peaks *a* to *c* (especially between C and C′), indicative of a change in polyphosphate chain length. It can be observed that the film formed is essentially a zinc polyphosphate glass.

figure 5(b) that the model zinc polyphosphate spectrum is shifted to higher energy from the unreacted ZDDP spectrum. Comparison of the surface (TEY) and bulk (FY) spectra of the standard film, and those formed on 52100 steel and A390 at shorter rubbing times and lower loads, indicates that a polyphosphate film has formed. A small shoulder labeled *s*, on the low energy side of peak 2 indicates that a small amount of unreacted ZDDP is found in the film. This would be expected since rubbing has only occurred for 10 min at 60 °C and a significant amount of ZDDP should remain unreacted in the solution. This would further indicate that the unreacted ZDDP must be trapped in the wear scar either in crevices or in the film. As was found with the P L-edge spectra, a comparison of aluminum to zinc polyphosphates revealed no significant differences and thus we were unable to distinguish one species of polyphosphate from the other, in the film. The K-edge FY spectrum of the A390 sample also agrees with the L-edge results, which indicate that the film is thin (identified by the low signal to noise ratio of the FY spectrum).

The P L- and K-edge results indicate the effectiveness of ZDDP as an antiwear additive. Even at low loads, and after a short rubbing-time ZDDP has decomposed thoroughly enough to create a relatively thick (50–100 nm) polyphosphate film on both the 52100 steel and A390 surfaces. Another significant observation relates the absence of either a phosphide signal or one originating from a linkage isomer. An aluminum phosphide species was previously found under low-load ZDDP boundary lubrication conditions on low Si content Al–Si alloys (0.7–7.0 wt.% Si) [40]. It was previously found to be the result of significant amounts of scuffing and wear of the aluminum matrix. This resulted in the fracturing of the aluminum oxide layer, and the wearing of aluminum asperities exposing nascent aluminum. Nascent aluminum was responsible for reacting with ZDDP forming intermediates and a phosphide species. In the present work there was no indication of either a peak at ~135.6 eV in the P L-edge spectra which would indicate the formation and presence of a linkage isomer species of ZDDP [40,65–67], or of a phosphide related signal at ~2145.5 eV in the P K-edge spectra. This would indicate that the amount of scuffing and/or wear of the aluminum matrix was limited, probably due to the presence and greater abundance (coverage) of larger Si grains which reduced the formation of the phosphide or intermediate species to below the detection limit of the spectroscopy. As was suggested in the earlier study [40], the introduction of the alloying Si element resulted in a *thicker* antiwear film. Thus, in this case, with a silicon content of ~18% the silicon grains must act as riders for the reciprocating steel pin and thus preventing severe wear and scuffing.

3.3. Micro-chemistry and nanomechanical properties of ZDDP antiwear films

3.3.1. ZDDP antiwear film on A390

Grid marks were placed on the samples after the antiwear tests were completed, which allowed for

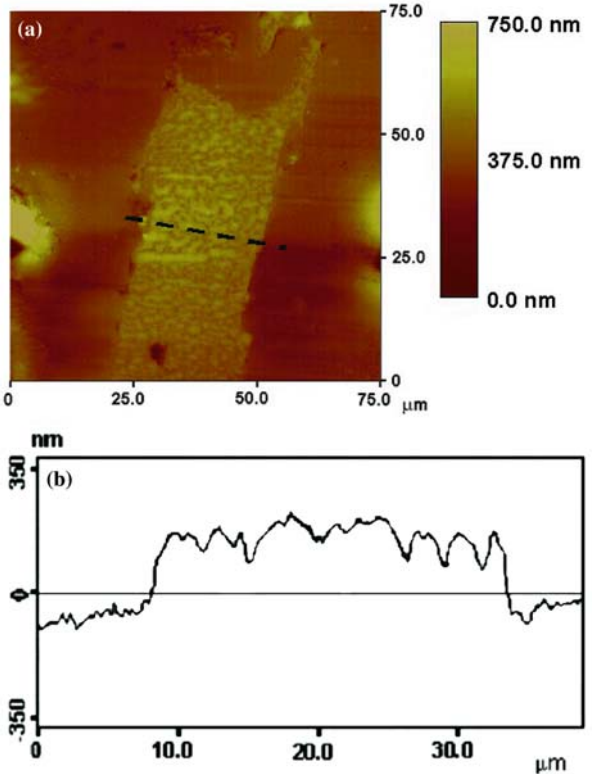

Figure 6. An AFM topography image of a representative silicon grain (a) for the 10 min rubbing-time film is shown. The antiwear pads can be observed as bright patches on the silicon grain (center). A cross-sectional analysis taken across the dashed line in (a) is shown in (b). Pads can be identified as bumps on the Si grain in the cross-sectional analysis.

relocation of the same features with all techniques. Figure 6(a) shows an AFM topography image of a large silicon grain in the aluminum matrix of an A390 sample. At the middle-left of the figure, a tip of one of the square grid-marks can just be observed. On close examination, small patches of antiwear film can be observed on the silicon grain. The patches are elongated in the direction of rubbing and are representative of what we term antiwear pads. This has been observed on steel surfaces [6,22–25,36]. Cross-section analysis of the grains allowed for approximate calculation of the height of the silicon grains, as well as the height of the antiwear pads formed on the silicon grains. A sectional analysis taken across the dashed line in figure 6(a) is shown in figure 6(b). The investigated grains, including antiwear film, were found to protrude from the matrix by up to 150–170 nm. The antiwear pads formed on the silicon grains were found to vary in thickness from anywhere between 30 and 100 nm.

Figure 7 shows SEM images and EDX maps for the antiwear film formed on A390, more specifically the silicon grain identified in figure 6. Figure 7(a) is a backscattered image showing an expanded view of the silicon grain of interest. The large grid marks can be identified around the region (identified by arrows). Figure 7(b) is a SEM field-emission image for the region outlined in figure 7(a). The large silicon grain can be found at the bottom-center of this image. One of the large grid marks can also be identified at the right of the image (figure 7(b)). The directionality of the rubbing can be easily observed in the image. The antiwear pads can be seen across the silicon particle and scuffing marks can be observed in the aluminum matrix corresponding to the rubbing direction. Figure 7(c)–(i) are elemental maps taken with 5.00 kV energy to enhance the *surface* sensitivity. Typically the K lines are the strongest X-ray emission lines that are used for elemental mapping, however at 5 kV the Zn L level is excited and provides a strong enough signal for our purpose. The silicon grains can be easily identified in the aluminum matrix. An interesting observation was made between location of zinc and the antiwear film formed on the silicon grains. Zinc was found to be concentrated in regions found on the Si grain. At the center of the silicon grain a large directionality to the zinc deposits can be found that corresponds to the antiwear pads (see AFM image; figure 6(a)). This agrees with the oxygen distribution, which shows a high locality of oxygen in the region of the antiwear pads. Thus the zinc and oxygen maps are consistent with the XANES results that describe the film as a zinc polyphosphate glass. Oxygen was also found through the Al-matrix and is assumed to be due to aluminum oxide.

Figure 8(a) shows the X-PEEM image of the silicon grain of interest. The X-PEEM image taken at 138.1 eV (peak *c* at the P L-edge). X-PEEM images are secondary electron images similar to those obtained by an SEM. The X-PEEM image shows the same silicon grain at the center of the image. The bright spots at the surface of the silicon grain are due to electrons emitted from the patches of antiwear film. Differences such as topography, shadowing, work function, and escape depth all contribute to the image. The P L-edge spectromicroscopy stack acquired for this region was analyzed thoroughly. Brightness in the image is due to a larger electron signal from the surface. Changes in the intensity of the signal can be due to charging, surface roughness, shadowing, etc. as well as due to changes in chemistry. It should be noted that the Al-matrix region was roughened due to the rubbing process and this has resulted in a mottled signal from the Al-matrix region showing bright spots which should not be mistaken as antiwear pads like those observed on the silicon grain. We have performed similar analysis on ZDDP films in previous studies [22,35]. Once the correlation between the topography images and the spectromicroscopy stacks were made, areas and selected features were chosen from which spectra were then extracted. As was briefly described above, regions of several pixels in size that

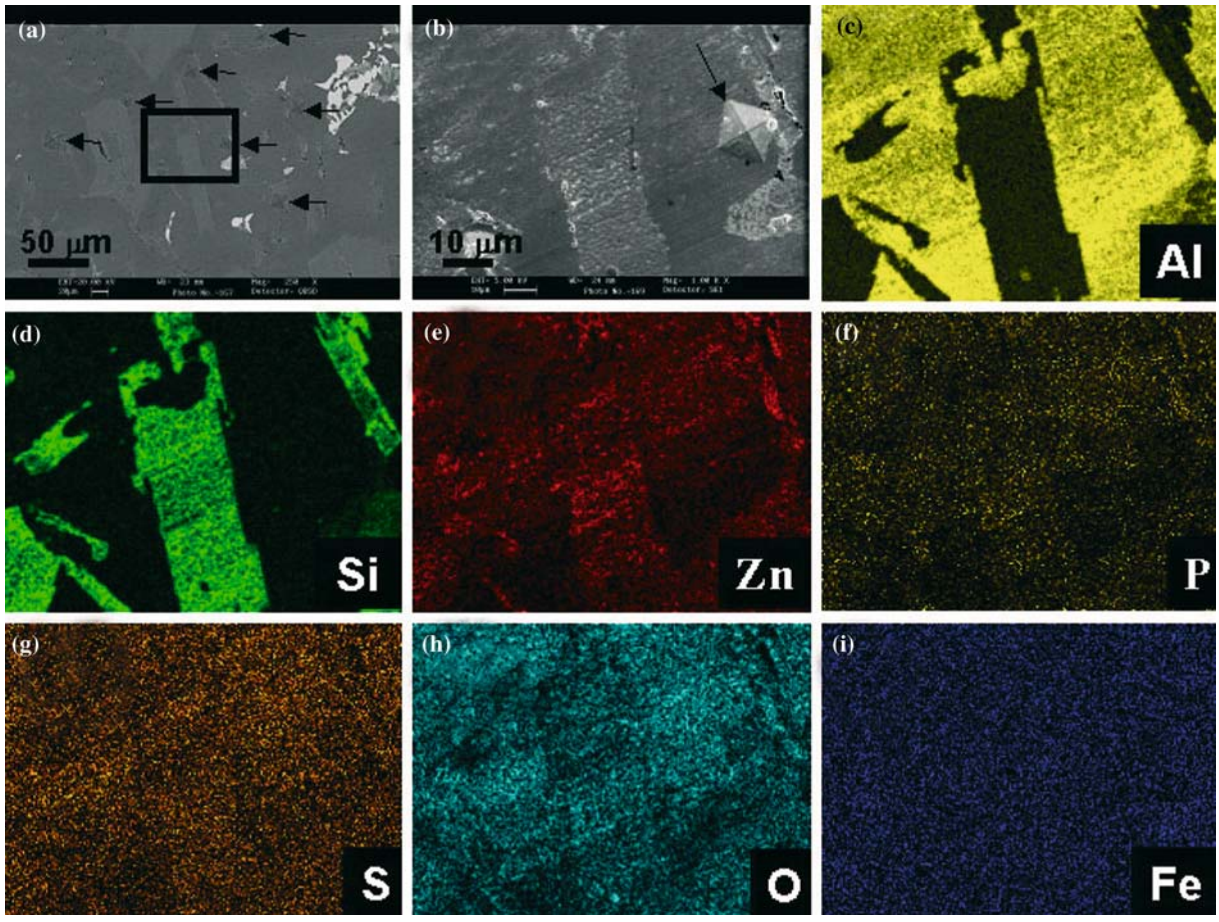

Figure 7. A backscattered SEM image is shown in (a). Arrows identify the grid marks used to re-locate specific features. A box outlines the location of image (b). Image (b) is a field-emission SEM image showing the silicon grain of interest (seen in figure 6) The corresponding EDX elemental maps (taken at 5 kV) are shown for aluminum (c), silicon (d), zinc (e), phosphorus (f), sulfur (g), oxygen (h) and iron (i). The bright contrast in images C–I indicates an abundance of the particular element. Localizations of zinc, phosphorus and oxygen can be observed on the silicon grain.

had interesting features such as high or low signal intensity, small pads, areas between antiwear pads, or areas on or off the silicon grains were examined. The spectra resulting from the selected regions are an average spectrum over all the pixels contained in the region. No identifiable differences in the extracted spectra were observed. Figure 8(a) shows two regions from which spectra were extracted. The resultant spectra are shown in figure 8(b). The P L-edge spectra extracted from the antiwear pads located on the silicon particle (spectrum D), and from the aluminum matrix (spectrum E) are compared to model spectra and unreacted ZDDP (spectrum A). First, as mentioned above, very little difference can be noted between the zinc and aluminum polyphosphates (the spectra contain peaks *a, b,* and *c* as well as similar intensities, although spectrum C was obtained with a higher eV resolution), making it difficult to distinguish the cation in the resultant film. The pads located on the silicon particle show the presence of a polyphosphate film. This film is essentially identical, chemically, to that formed on steel surfaces [6,22,24,26,29,35]. A small shoulder, labeled *s*, at the low energy side of peak *a* is due to unreacted ZDDP. This indicates that ZDDP is still found in the contact zone during such short rubbing times and low loads. This also suggests that the unreacted ZDDP may be trapped in the valleys between the antiwear pads, or embedded into the surface of antiwear pads. This is beneficial since unreacted ZDDP can then decompose and replenish the polyphosphate film when it wears away. Surprisingly, since no visible patches of film were found using the AFM or SEM, polyphosphate spectra were also obtained from the matrix region (spectrum E). However this spectrum had more intense peaks for unreacted ZDDP. There is no direct evidence, through topographic imaging, to support a theory suggesting that the polyphosphate film has been directly formed on the aluminum matrix and remains there. It might then be inferred that the polyphosphate glass found in the matrix regions was transferred from the silicon grains during rubbing. Furthermore, the resultant transfer has not formed any large or small pads visible on the surface. This would be consistent with the smaller thickness (<5 nm; the detection limit

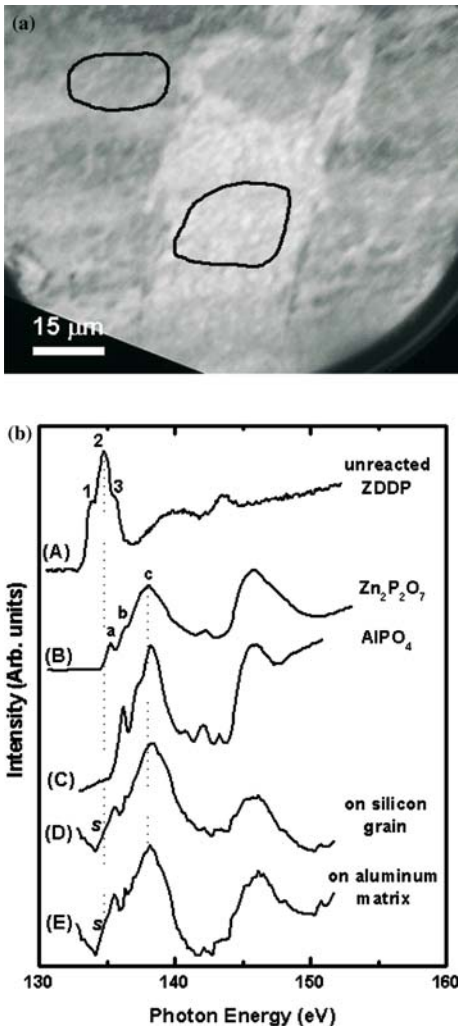

Figure 8. A secondary electron image, obtained by the X-PEEM, of the silicon grain is shown in (a), taken at 138.1 eV; which corresponds to peak c in the P L-edge spectra) and the corresponding spectra extracted from the outlined regions are shown in (b). The P L-edge spectra obtained from the silicon grain (spectrum D) and Al-matrix (spectrum E) are compared to model zinc (spectrum B) and aluminum (spectrum C) polyphosphates. Polyphosphate can be observed on both the Al-matrix and on the silicon grain.

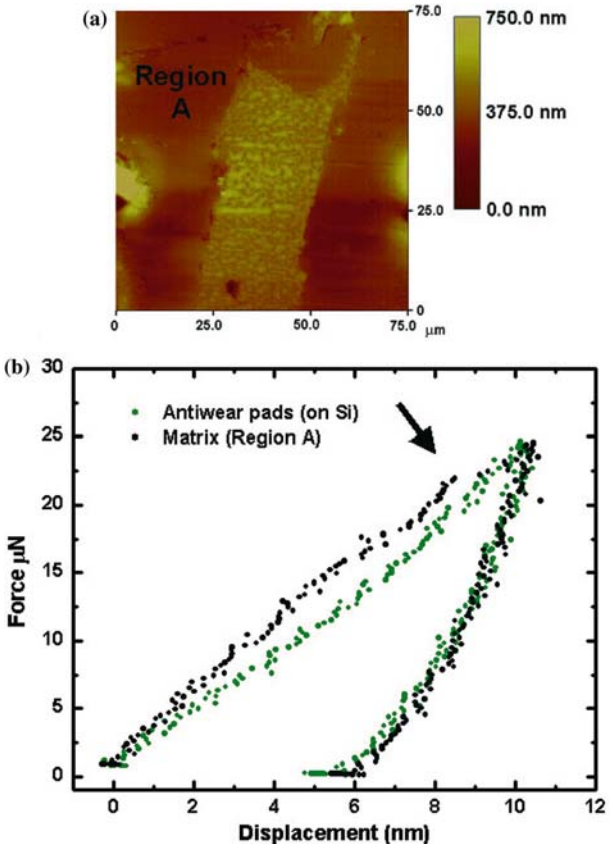

Figure 9. Antiwear pads can be observed on the surface of the silicon grain in the AFM topography image (a). The pads appear as bright patches in the image. *f–d* curves were taken in Region A, and on the antiwear pads on the silicon grain. Representative *f–d* curves are shown in (b). Dislocations in the loading-curve of the Al-matrix are indicative of aluminum oxide fracturing (shown by arrows).

of X-PEEM) of the films on the matrix compared to that on the silicon grains as was observed as a poor signal-to-noise ratio of the TEY, X-PEEM spectra taken from the matrix regions compared to that from the silicon grains.

Nanomechanical measurements of the antiwear pads on this silicon grain were also made. Several *f–d* curves were recorded to a maximum load of 25 μN on the larger pads. The heights of the measured pads were determined by cross-sectional analysis of the AFM topography images (see figure 6(b) for example). AFM cross-sectional analysis was used to determine the approximate thickness of the antiwear pads. The average thickness of the pads was measured to be ~80 nm. Figure 9(a) shows an AFM topography image of the silicon grain and surrounding aluminum matrix. The average E_s* value was calculated from the *f–d* curves, taken on several antiwear pads on the Si grain. Since the approximated thickness of the antiwear pads was *known*, from the AFM topography image, maximum loads used for the indentations were kept low enough to maintain a maximum penetration of ~10% of the film thickness. The average E_s* value was calculated to be 76 ± 7 GPa. Assuming that the stiffness of the silicon grain may have influenced the elastic response of the film, the E_s* value was corrected using the Song and Pharr method [52] and the approximate film thickness of each of the antiwear pads measured by AFM. All values are further listed in table 1 for comparison purposes. The modulus of the film (E_f) was calculated to be 66 ± 7 GPa.

f–d curves were also measured in the matrix (Region A in figure 9(a)). The indentation modulus (E_s*) was calculated to be 71 ± 9 GPa. This value is much lower than that measured for the matrix of a blank polished A390 sample (129 ± 15 GPa, see section 3.1). There are two reasons that may explain this effect. Firstly, with rubbing, the thick aluminum oxide layer may have been removed and replaced with a thinner

layer, which may not have influenced the *f–d* curves as significantly. Indeed, Figure 4 showed that the oxide layer is substantially thinner in the sample after rubbing, compared to the untreated specimen. Secondly, due to the low penetrating *f–d* curves taken in this region (to maintain a comparison to the *f–d* curves taken on the ZDDP films), the roughness of the surface may have been influencing the modulus in this region.

Representative *f–d* curves for the antiwear pads found on the silicon grains and for the matrix region are shown in figure 9(b). Comparison of the hysteresis of the indentation curves of that of a bare silicon grain (see figure 2) to that of the indentation curve taken on the antiwear film indicates that they have a similar elastic response. However, a difference in hysteresis indicates that under low loads, the silicon grain *fully* recovers from the indentation process, and that plastic deformation occurs in the antiwear pads. Thus, at these loads the silicon grain is much more elastic than the antiwear film. Graham *et al.* [25] found a lower indentation modulus for the small antiwear pads formed on a steel substrate compared to those measured for the large antiwear pads. Their value of 74 ± 20 GPa is within experimental error of the values we have measured for the small antiwear pads formed on the silicon grains. Figure 9(b) also shows a dislocation in the aluminum matrix *f–d* curves (indicated by arrow). These dislocations can be due to the oxide layer, as well as the detection of the surface roughness at such low loads.

3.3.2. ZDDP antiwear film on 52100 steel

For comparison purposes, a similar investigation was performed on an antiwear film formed on steel under the same rubbing conditions. Figure 10(a) shows an AFM topography image of a selected region of interest with two major zones of interest. The first is located at the top of the image, which shows primarily scuffing due to the reciprocating pin. The second region, covers from the center of the image downward, in which the reciprocating contact gradually increased along with film formation. Large, elongated antiwear streaks can be observed. The streaks are elongated in the rubbing direction. Figure 10(b) shows an AFM cross-sectional analysis that was taken across the dashed line in figure 10(a). Streaks are numbered 1–3 for purposes of orientation, and identification in the following results. AFM cross-sectional analysis was used to determine the thickness of the antiwear streaks. On average the streaks that were measured had a thickness between 110 and 140 nm. The film thickness for a particular antiwear pad was determined by taking a conservative approach. The pad thickness was measured from halfway up the vertical rise for the antiwear pad, to its top, as observed in the line profiles. A P L-edge spectromicroscopy stack was

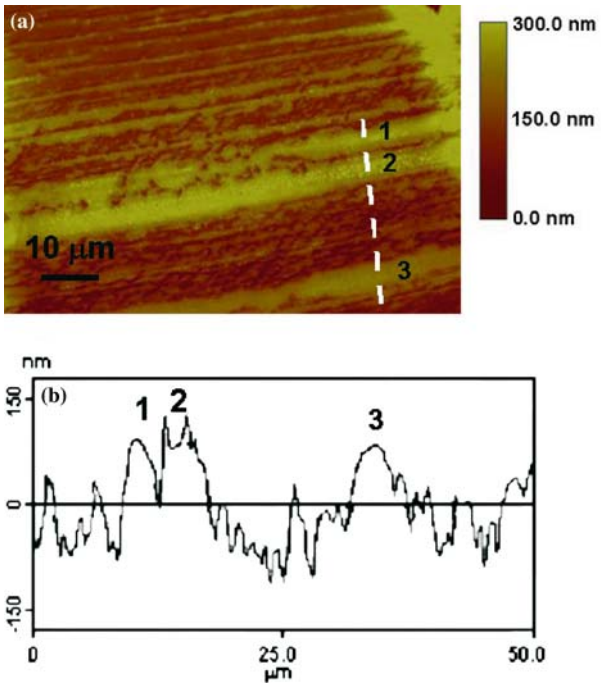

Figure 10. An AFM topography image of a representative area on the 52100 steel sample (10 min rubbing-time) is shown (a). Numbers are added for orientation purposes. Antiwear pads (streaks) can be observed along the surface. The streaks appear as bright lines across the image. An AFM cross-sectional analysis taken across the dashed line in (a) is shown in (b). The orientation numbers can identify the antiwear pads.

acquired for this region. Analysis of the different features is shown in figure 11. Figure 11(a) is an X-PEEM image taken at 138.1 eV. Due to shadowing, and charging of the thicker antiwear film, the elongated antiwear streaks appear as dark streaks across the X-PEEM image. Spectra were extracted from the regions outlined in figure 11(a). The corresponding spectra are shown in figure 11(b), and are the average spectrum from all pixels within an outlined region. The spectra are compared to unreacted ZDDP and a model zinc polyphosphate. It can be observed for region 1 (the scuffing zone) that a significant amount of unreacted ZDDP is present (shoulder *s*). Furthermore, there is some polyphosphate film formation. Due to a low relative peak height ratio of peaks *a:c*, it can be concluded that short-chain polyphosphates are located in this area. Regions 2, 4, and 6 are spectra on the elongated antiwear streaks, and are very similar to the model zinc polyphosphate glass spectrum. This indicates that in the higher load regions, ZDDP has decomposed and formed the protective antiwear film, resulting in the formation of the streaks. The polyphosphate chain length is longer than that found in zone 1. Region 3 is located between streaks 1 and 2 (see figure 10(a)) and the spectrum shows a polyphosphate film with some unreacted ZDDP (small shoulder *s*). This result has been found in previous studies [16,22,35], which suggest that ZDDP is trapped

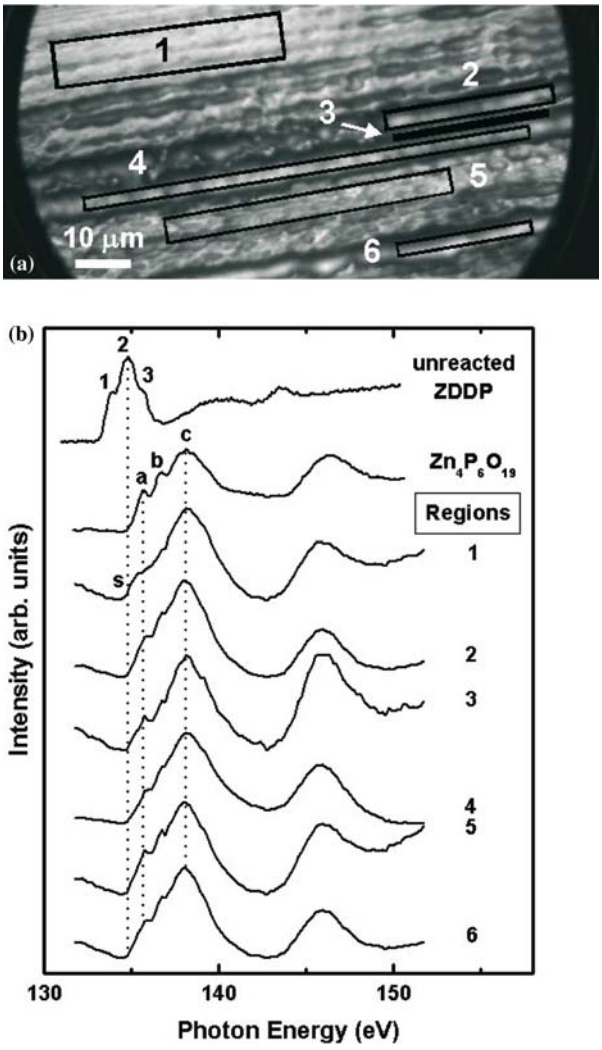

Figure 11. P L-edge XANES spectra were extracted from the areas outlined in the X-PEEM image (a). The regions are numbered to identify the corresponding spectra in (b). In most cases the film was chemically identical, and consistent with a zinc polyphosphate glass. Region 1, where there was intermittent contact, shows more unreacted ZDDP.

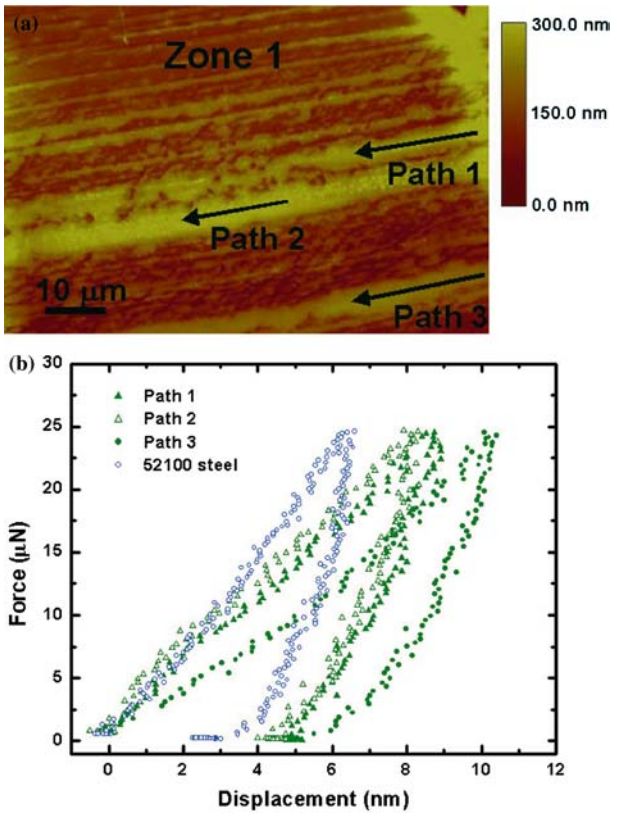

Figure 12. An AFM topography image shows the antiwear streaks and the paths along which several *f–d* curves were taken (a) on the 10 min film. Numbers are added to help in identifying particular streaks of interest. Representative *f–d* curves taken from each path are shown in (b) and compared to a *f–d* curve taken into blank 52100 steel.

in valleys that act like reservoirs to replenish the film as it wears away.

The nanoscale mechanical properties of the antiwear streaks were measured by nanoindentation. Several areas were examined and shown on the AFM topography image in figure 12(a). Multiple *f–d* curves, taken to a maximum load of 25 μN, were measured in zone 1 and along paths 1–3. The average E_s* calculated from the *f–d* curves taken in zone 1 was 194 ± 26 GPa. The large scatter is the result of the error in calculating the E* value for force curves taken to a maximum load of 25 μN in steel (total penetration of <10 nm) and those with calculating the tip area function at low penetration depths. The scatter is also the result of the roughness of the surface in this area. Another explanation may be that the thin antiwear film (detected by X-PEEM, see figure 11(b), spectrum 1) located in this region may be influencing the mechanical response and thus lowering the value from that expected for steel. Multiple indents were taken along paths 1–3, the indentation moduli, E_s*, and corrected E_f values are listed in table 1. The E_s* values were corrected using the Song and Pharr method [52] to compensate for the effect of the underlying steel substrate on the elastic response of the antiwear film. These values are in close agreement with those found previously for ZDDP antiwear pads formed on steel surfaces at higher loads (220 N) and longer rubbing times (1 h) [6,22,24,25,35]. Representative *f–d* curves for the different antiwear streaks are shown in figure 12(b). The *f–d* curves are compared to one taken in polished 52100 steel, at the same maximum indentation-load. It can be observed that the hysteresis in the *f–d* curves taken on the antiwear streaks is slightly larger than that for the polished steel substrate. This indicates that the film has a larger plastic response than the steel substrate. Furthermore, on examination of the initial portion of the withdrawal curves, it can be seen that the steel substrate has a steeper slope indicative a stiffer response than the antiwear streaks. This was observed previously on the

Table 1.
The areas examined on the 10 min rubbing-time films formed on A390 and 52100 steel.

Areas examined after 10 min rubbing		Number of curves averaged	E_s* (GPa)	E_f (GPa)
A390 sample	Pads on Si grain	32	76 ± 7	66 ± 7
	Al matrix	13	71 ± 9	–
52100 steel	Zone 1	14	194 ± 26	–
sample	Path 1	6	94 ± 3	86 ± 3
	Path 2	14	112 ± 7	103 ± 7
	Path 3	30	78 ± 8	70 ± 8

The number of curves used to produce the error (2σ) in the calculated values are listed along with the indentation moduli (E_s*) and corrected moduili (E_f) for the specified locations.

silicon grain thus indicating that the films (on different substrates) have a similar elastic response.

The values obtained for the antiwear streaks are slightly higher than those measured for the antiwear pads on the silicon particle (see above). An explanation for this can be the result of several effects. The first is due to the physical mechanism of film formation and the mechanical properties of materials involved. It has been previously found that the nanoscale mechanical properties of ZDDP antiwear pads have a heterogeneity in which the center of the pads have a stiffer and more elastic response than the edges of a pad [6,25]. It was suggested that this is due to the higher shear forces and loads experienced at the center of the pads than at the edges, which result in a larger pressure (at the center) which may be responsible for changing the networking (bonding) in the polyphosphate glass [22,25]. Using this same hypothesis, we suggest that conformation between two rubbing 52100 steel surfaces is much greater than that between A390 coupon and a 52100 steel pin. In the 52100 steel system the polished surface of the coupon and the edge of the pin conform very well, yet in the A390/52100 couple the steel pin rides (primarily) across the top of the silicon grains only having intermittent contact with the Al-matrix. This results in larger forces (in the 52100 couple) and a transformation of the polyphosphate glass, resulting in a slightly higher elastic response. In the A390/52100 couple, the reciprocating pin is being constantly scraped by the protruding silicon grains on the A390 surface. This does not allow for the efficient build-up of polyphosphate film on either surface.

3.4. Macro-XANES analysis at the P L- and K-edge, extended rubbing time

The results reported above were all for 10 min rubbing times. It is of interest to determine if any changes occur in the spatially resolved chemical, physical (morphological), and mechanical properties of the AW films at longer (60 min) rubbing times, at 60 °C, 25 Hz and 60 N load.

P L-edge results (not shown) indicated that under the test conditions ZDDP has decomposed, and that the AW films formed on 52100 steel and A390 have XANES spectra that are essentially identical to the zinc polyphosphate ($Zn_4P_6O_{19}$). The spectra show that the film is composed of shorter-chain polyphosphates in the bulk and slightly longer polyphosphates at the surface. This was most evident in the spectra obtained from the A390 sample (60 min rubbing-time). The spectra are identical to those observed for the 10 min rubbing-time films for the A390 sample (see figure 5(a), spectra C and C′) and thus are not shown.

The P K-edge results (not shown) agree closely with those of the P L-edge for the 60 min films. The spectra showed that the film formed is essentially a zinc polyphosphate. Poor signal-to-noise ratio for the FY spectrum taken of the AW film formed on A390 indicates that the film is thin. Also of interest, was a lack of a pre-edge peak at ~2145.5 eV and one at 2150.1 eV. These two peaks were observed on worn aluminum surfaces and attributed to the formation of aluminum phosphide (P^{3-}) and a linkage isomer of ZDDP [40]. This indicates that the large silicon grains must be acting like riders preventing a significant amount of aluminum wear and the formation of phosphide and linkage isomer species of ZDDP.

3.5. Micro-chemistry and nanomechanical properties of ZDDP antiwear films

3.5.1. ZDDP antiwear film on A390

Figure 13(a) shows an X-PEEM image taken at 138.2 eV (peak c of the P L-edge). There are many contributions to the signal generation process—chemistry, topography, shadowing, and charging to name a few. At the center of the image is a large silicon grain, atop which large antiwear pads can be observed as dark patches. The silicon grain and antiwear pads are much more visible in the AFM height image (figure 13(b)). An elongation of the antiwear pads in an up-down direction is indication of the rubbing direction. Silicon grains were measured by AFM

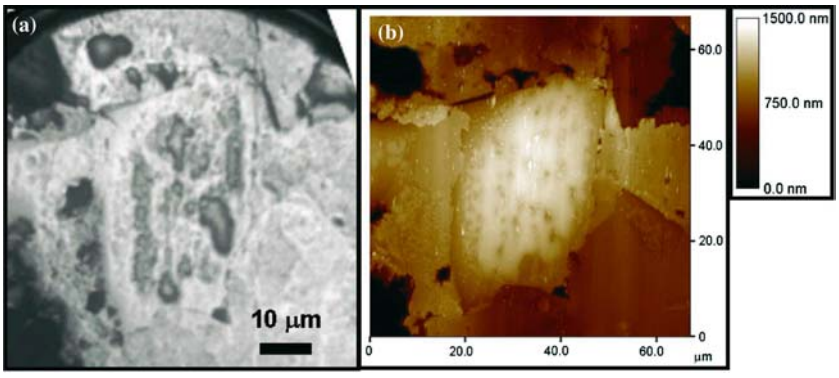

Figure 13. An X-PEEM image (taken at 138.1 eV) shows a typical silicon grain, observed in the center of the image, for the A390 surface after 60 min rubbing (a). The streaks are shaded due to shadowing and charging. The corresponding AFM topography image is shown in (b). Large antiwear pads can be observed on the silicon grain. No pads were identified on the Al-matrix.

cross-sectional analysis to be raised from the aluminum matrix by >150 nm. The antiwear pads were determined, by the same procedure, to be extended from the surface of the silicon grains by 150–250 nm. These antiwear pads are much thicker, and larger in volume, than that found for shorter-rubbing times. This is an indication that the film does in fact grow with rubbing time. No visible antiwear pads were detected by AFM on the Al-matrix. Other features that can be observed in the images, are large pores formed by gas that is introduced during the casting process.

P L-edge spectra (not shown) extracted from localized regions of the silicon grain and Al-matrix showed a small amount of unreacted ZDDP. It is important to note, that on the silicon grains, the polyphosphate signal was much greater than in the matrix area. These spectra agree with what was found by the macro-scale XANES analysis (see section 3.2) but provide more detail about the spatial chemistry in the film on the micro-scale.

Force imaging was performed using the Hysitron force transducer®, of the same silicon grain using a stiffness imaging approach [68–71]. Elastic modulus imaging (force imaging) was performed by applying a sinusoidal force to the diamond tip to introduce an oscillation, ''tapping mode''. Data were acquired and processed to obtain contact force, sinusoidal displacement amplitude and phase shift, using a lock-in amplifier, as the tip scans across the surface. The contact stiffness is calculated from the amplitude and phase shift using a dynamic model, which takes into account the system mechanics such as mass, spring constant, and damping loss, as well as instrument compliance [68–71]. Appropriate contact models, tip geometry, and system electronic corrections were used to process the data [68–71]. The result is the quantitative measurement (mapping) of the elastic modulus through stiffness measurements. Modulation to the tip consisted of a sinusoidal force of 3.99 μN at 500 Hz. The tip velocity was maintained at 16 μm/s. This resulted in a tip displacement of 18 nm. The lock-in time constant was set to 100 μs. Analysis of the antiwear pads atop the silicon grain gave a modulus of ~50–65 GPa. However there was some error in this measurement due to ringing of the collection signal [68–71]. Nonetheless this value is similar to what was measured previously for shorter rubbing times on silicon grains on A390.

3.5.2. ZDDP antiwear film on 52100 steel

An AFM height image of a selected region is shown in figure 14. The region has two areas of interest. The first is located at the top of the image that shows that intermittent contact had occurred between the steel sample and that reciprocating pin. There is very little film formation and scuffing is observed on the steel surface. The second area is the large antiwear pad found in the lower quadrant of the image. These quadrants are similar to those identified for the 10-min

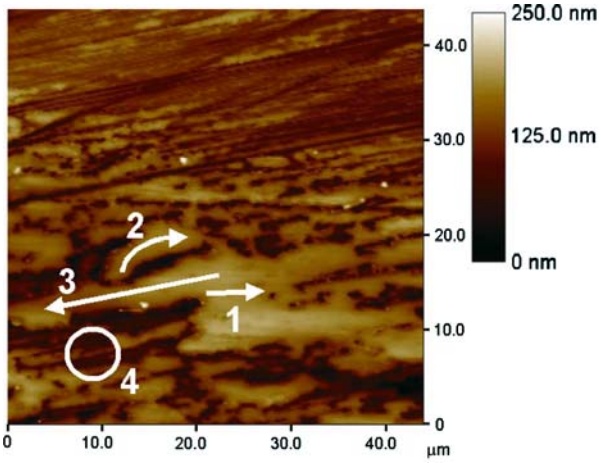

Figure 14. An AFM topography image of the antiwear film formed on 52100 steel after 60 min rubbing is shown. The paths (and area) along which several *f–d* curves were taken is also shown. A quadrant with intermittent contact can be observed at the top of the image. Larger antiwear pads are located at the bottom of the image.

Table 2.
The areas examined on the 60 min rubbing-time films formed on A390 and 52100 steel. The number of curves used to produce the error (2σ) in the calculated values are listed along with the estimated film thickness, indentation moduli (E_s*) and corrected moduili (E_f) for the specified locations.

	Path	No. of curves averaged	E_s* (GPa)	Film thickness (nm)	E_f (GPa)
A390 sample	Pads on Si grain	–	50–65[†]		
52100 steel	1	10	110 ± 8	85	98 ± 7
sample	2	19	110 ± 7	81	98 ± 7
	3	7	97 ± 7	71	87 ± 7
	4	12	>250	–	–

[†]The values determined for the pads on the silicon grain for the A390 sample was determined by force imaging (see text).

rubbing-time film on 52100 steel. It can be observed that the antiwear pads are much longer and cover a greater surface area than that observed for the short rubbing-time. The P L-edge XANES spectra were extracted using the X-PEEM analysis procedure. Areas were selected in and around the antiwear pads as well as in the intermittent contact area. It was found that the antiwear pads have a bilayer structure with shorter-chain polyphosphates and the substrate interface, and longer-chain polyphosphates found at the surface. A small amount of unreacted ZDDP was also found. It was found that in the areas between the large pads and in quadrant 1 (the intermittent contact zone) there was very little phosphate signal.

Figure 14 also shows the paths along which a series of indents were performed. A series of nanoindentation experiments were taken to maximum loads between 30–40 μN. The values are listed in table 2 along with the number of indents averaged for each path taken. Also listed are the corrected values using the Song and Pharr method [52]. This method requires the thickness of the film to be known. AFM cross-sectional analysis was used to determine the approximate thickness of the antiwear pads. The pads measured by nanoindentation, were found to have a thickness between 70 and 85 nm. It can be observed that these values are in close agreement with those found previously for ZDDP antiwear pads formed at short rubbing times and to those formed on steel surfaces at higher loads (220 N) and longer rubbing times (1 h) [6,22,24,25,35]. The large values measured for area 4 is the result calculation errors for f–d curves with low penetration depths. The f–d curves taken to 40 μN in region 4 (comparable to bare steel) had very low penetration depths and thus difficulties in determining the tip area function. The scatter is also the result of the roughness of the surface in this area.

7. Conclusions

A comparison has been made of ZDDP antiwear films formed on the Al alloy (A390) with those formed on 52100 steel under the same rubbing conditions. The conditions applied in the antiwear tests are similar to those experienced at the cylinder/bore wall in a combustion engine (lower load). Antiwear films formed during the initial stages of wear (10 min) were also compared to those formed at prolonged rubbing times (60 min). The first nanoscale chemical and mechanical comparison of antiwear pads formed on both surfaces, and both rubbing times, has been performed. This study has shown, for the first time, the location of antiwear film formation on high silicon-content Al–Si alloys. The following general conclusions can be drawn from the results presented above:

1. Macro-scale chemical analysis has shown that oxides, of both aluminum and silicon, have been formed on the surface of A390 after rubbing. The appearance of a fairly thick zinc polyphosphate film has been found on all surfaces (10 and 60-min rubbing films). The chemical nature of the polyphosphate spectra (shorter-chain length), on the 52100 steel sample (10 min rubbing-time), differs from that found on steel surfaces for longer rubbing times [15,16,19,22] which produce a bilayer structure with longer-chain polyphosphates at the surface and shorter-chain in the bulk. The polyphosphate spectra obtained on both A390 surfaces are essentially identical. The bilayer structure was observed on the A390 surfaces at both short and long rubbing-times.
2. X-PEEM micro-chemical analysis agreed closely with those found on the macro-scale. However, of more interest, was the spatially resolved chemistry found on the A390 surface. X-PEEM analysis has shown that the polyphosphate film is present on both the matrix and the silicon grains, and is identical in chemical nature. The spectra show a zinc polyphosphate structure. However, limitations in the ability to distinguish aluminum polyphosphate from zinc polyphosphate cannot exclude the fact that aluminum cations may also be intermixed with the zinc cations.
3. AFM, SEM, and X-PEEM imaging has shown that ZDDP antiwear pads form mainly on the silicon grains. These pads are very similar to those formed on steel. Since the silicon grains protrude from the

surface of the aluminum matrix, it is natural to suppose that the load was carried by these grains and not by the matrix. For the longer-rubbing times the antiwear pads were found to be larger in volume than that found for shorter-rubbing times. This is an indication that the film does in fact grow with increased rubbing time.

4. The modulus for the antiwear pads (on steel surface) is within experimental error of that found for films formed at higher loads and temperatures [6,22,24,25,35]. The antiwear pads located on the silicon grains have a slightly lower modulus than those found for the large antiwear pads on steel surfaces [6,22,24–29,35]. However, these values are in close agreement with those found for small antiwear pads ($<8\ \mu m^2$ in size) found on steel surfaces by Graham et al [25]. This suggests that the films are essentially identical, in terms of nanomechanical response, from the onset of formation.

This evidence is beneficial to understanding the applicability of such an alloy at the cylinder/bore interface. This provides new insight into the wear processes on high silicon content Al–Si alloys, at low loads, and provides detailed information about the performance of A390 lubrication process.

Acknowledgments

M.A.N. would like to personally thank A.P. Hitchcock for his help with aXis2000 and useful discussions about the analysis of the X-PEEM data. The authors would also like to thank K. Tan, A. Jurgensen, from Canadian Synchrotron Radiation Facility (CSRF) and to the staff of the Synchrotron Radiation Center (SRC), University of Wisconsin, Madison, for their technical support and the National Science Foundation (NSF) for supporting the SRC under Award #DMR-0084402. The authors would like to thank Yang-Tse Cheng, Weston Capehart, and Thomas Perry of General Motors, Warren MI, for the supply of the aluminum 390 alloy and their interest, and Imperial Oil (Sarnia Ontario, Canada) for the ZDDP concentrate. We are also grateful to Heather Bloomfield and Ross Davidson of Surface Science Western, University of Western Ontario, for discussions about the SEM and EDX results. This work was financially supported by the National Research Council of Canada (NRC), and the Natural Sciences and Engineering Research Council of Canada (NSERC), General Motors of Canada Ltd, and Hysitron Inc.

References

[1] L.E. Reuss and C.N. Hughes, SAE Congress 710150 (1971) 577.
[2] F.J. Kneisler, D.A. Martens and R.W. Midgley, SAE Congress, (1971) 520.
[3] M. Platt, J. Auto. Eng. (1971) 3.
[4] Z. Zurecki, D. Garg and D. Bowe, Suf. Eng. 12 (1996) 217.
[5] A. Edrisy, T. Perry, Y.T. Cheng and A.T. Alpas, Wear 250–251 (2001) 1023.
[6] M.A. Nicholls, T. Do, P.R. Norton, G.M. Bancroft, M. Kasrai, T.W. Capehart, Y.-T. Cheng and T. Perry, Tribol. Lett. 15 (2003) 241.
[7] D.M. Jacobson and A.J. W. Ogilvy, Mat.-wiss. u. Werkstofftech. 34 (2003) 381.
[8] J.S. Sheasby, T.A. Caughlin and W.A. Mackwood, Wear 201 (1996) 209.
[9] J.S. Sheasby, T.A. Caughlin and W.A. Mackwood, Wear 196 (1996) 100.
[10] C. Grossiord, J.M. Martin, T. Le Mogne and T. Palermo, Tribal Lett. 6 (1999) 171.
[11] Q.J. Xue and M.W. Bai, Wear 195 (1996) 66.
[12] J.M. Martin, J.L. Mansot, I. Berbezier and H. Dexpert, Wear 93 (1984) 117.
[13] J.C. Bell and K.M. Delargy, in: The 6th International Congress on Tribology (“Eurotrib ’93”, 1993).
[14] M. Fuller, Z. Yin, M. Kasrai, G.M. Bancroft, E.S. Yamaguchi, P.R. Ryason, P.A. Willermet and K.H. Tan, Tribol. Int. 30 (1997) 305.
[15] G.M. Bancroft, M. Kasrai, M. Fuller, Z. Yin, K. Fyfe and K.H. Tan, Tribol. Lett. 3 (1997) 47.
[16] Z. Yin, M. Kasrai, M. Fuller, G.M. Bancroft, K. Fyfe and K.H. Tan, Wear 202 (1997) 172.
[17] E.S. Ferrari, K.J. Roberts and D. Adams, Wear 236 (1999) 246.
[18] E.S. Ferrari, K.J. Roberts and D. Adams, Wear 253 (2002) 759.
[19] M. Fuller, Z. Yin, M. Kasrai, G.M. Bancroft, K. Fyfe and K.H. Tan, in: *Proceedings of International Tribology Conference, Yokohama, 1995*, Vol. 2, (Japanese Society of Tribology, Tokyo, 1996) 1113.
[20] Z. Yin, M. Kasrai, G.M. Bancroft, K.F. Laycock and K.H. Tan, Tribol. Int. 26 (1993) 383.
[21] M. Kasrai, M. Fuller, M. Scaini, Z. Yin, R.W. Brunner, G.M. Bancroft, M.E. Fleet, K. Fyfe and K.H. Tan, in: *Lubricants and Lubrication: Lubrication at the Frontier*, Vol. 30, eds. D. Dowson, et al. (Elsevier Science B.V., Amsterdam, 1995) 659.
[22] M.A. Nicholls, P.R. Norton, G.M. Bancroft, M. Kasrai, T. Do, B.H. Fraser and G. De Stasio, Tribol. Lett. 17 (2004) 205.
[23] A.J. Pidduck and G.C. Smith, Wear 212 (1997) 254.
[24] O.L. Warren, J.F. Graham, P.R. Norton, J.E. Houston and T.A. Michalske, Tribol. Lett. 4 (1998) 189.
[25] J.F. Graham, C. McCague and P.R. Norton, Tribol. Lett. 6 (1999) 149.
[26] S. Bec and A. Tonck, in: *Tribology Series: Lubricants and Lubrication*, Vol. 30, eds. D. Dowson, C. Taylor, T. Childs and G. Dalmaz (Elsevier, Amsterdam, 1996) 173.
[27] S. Bec, A. Tonck, J.M. Georges, R.C. Coy, J.C. Bell and G.W. Roper, Proc. Roy. Soc. Lond. A. 455 (1999) 4181.
[28] M. Aktary, M.T. McDermott and G.A. McAlpine, Tribol. Lett. 12 (2002) 155.
[29] J. Ye, M. Kano and Y. Yasuda, Tribol. Lett. 13 (2002) 41.
[30] C. Jacobsen, S. Wirick, G. Flynn and C. Zimba, J. Micros. 197 (2000) 173.
[31] C. Morin, H. Ikeura-Sekiguchi, T. Tyliszczak, R. Cornelius, J.L. Brash, A.P. Hitchcock, A. Scholl, F. Nolting, G. Appel, D.A. Winesett, K. Kaznacheyev and H. Ade, J. Elect. Spectrosc. Rel. Phen. 121 (2001) 203.
[32] I.N. Koprinarov, A.P. Hitchcock, C.T. McCrory and R.F. Childs, J. Phys. Chem. B. 106 (2002) 5358.
[33] J. Stohr and S. Anders, IBM J. Res. Develop. 44 (2000) 535.
[34] G.W. Canning, M.L. Fuller, G.M. Bancroft, M. Kasrai, J.N. Cutler, G. De Stasio and B. Gilbert, Tribol. Lett. 6 (1999) 159.
[35] M.A. Nicholls, G.M. Bancroft, P.R. Norton, M. Kasrai, G. De Stasio, B.H. Frazer and L.M. Wiese, Tribol. Lett. 17 (2004) 245.

[36] A. Tonck, S. Bec, J.M. Georges, R.C. Coy, J.C. Bell and G.W. Roper, in: *Tribology Series: Lubrication at the Frontier*, Vol. 36, ed. D. Dowson (Elsevier Science B.V., Amsterdam, 1999) 39.
[37] T. Konishi, E.E. Klaus and J.L. Duda, Tribol Trans. 39 (1996) 811.
[38] Y. Wan, L.L. Cao and Q.J. Xue, Tribol. Int. 30 (1997) 767.
[39] M. Fuller, M. Kasrai, J.S. Sheasby, G.M. Bancroft, K. Fyfe and K.H. Tan, Tribol. Lett. 1 (1995) 367.
[40] M.A. Nicholls, P.R. Norton, G.M. Bancroft and M. Kasrai, Wear 257 (2004) 311.
[41] U. Wallfahrer and L. Bowen, J. Soc. Tribol. Lubricat. Eng. 53 (1997) 23.
[42] W.C. Oliver and G.M. Pharr, J. Mater. Res. 7 (1992) 1564.
[43] A.V. Kulkarni and B. Bhushan, Mater. Lett. 29 (1996) 221.
[44] M.F. Doerner and W.D. Nix, J. Mater. Res. 1 (1986) 601.
[45] J. Malzbender and G. de With, Surf. Coat. Technol. 135 (2000) 60.
[46] T. Chudoba, N. Schawarzer and F. Richter, Surf. Coat. Technol. 127 (2000) 9.
[47] G.M. Pharr and W.C. Oliver, MRS Bull. 17 (1992) 28.
[48] A.M. Korsunsky, M.R. McGurk, S.J. Bull and T.F. Page, Surf. Coat. Technol. 99 (1998) 171.
[49] T. Chudoba, N. Schwarzer, F. Richter and U. Beck, Thin Solid Films 377–378 (2000) 366.
[50] J. Malzbender and G. de With, Surf. Coat. Technol. 127 (2000) 266.
[51] S. Bec, A. Tonck, J.-M. Georges and J.-L. Loubet, Phil. Mag. A 74 (1996) 1061.
[52] A. Rar, H. Song and G.M. Pharr, in: *Materials Research Society Symposium Proceedings, Thin Films: Stresses and Mechanical Properties IX*, Vol. 695, eds. C.S. Ozkan, L.B. Freund, R.C. Cammarata and H. Gao (Materials Research Society, Warrendale, PA, 2002) 431.
[53] H. Gao, C.-H. Chiu and J. Lee, Int. J. Solids Struct. 29 (1992) 2471.
[54] M. Kasrai, Z. Yin, G.M. Bancroft and K. Tan, J. Vac. Sci. Technol. A 11 (1993) 2694.
[55] B.H. Frazer, M. Girasole, L.M. Wiese, T. Franz and G. De Stasio, *Ultramicroscopy* 99 (2003) 87.
[56] B.H. Frazer, B. Gilbert, B.R. Sonderegger and G. De Stasio, Surf. Sci. 537 (2003) 161.
[57] M. Kasrai, W.N. Lennard, R.W. Brunner, G.M. Bancroft, J.A. Bardwell and K.H. Tan, Appl. Surf. Sci. 99 (1996) 303.
[58] L.M. Croll, J.F. Britten, C. Morin, A.P. Hitchcock and H.D. H. Stoever, J. Synchro. Rad. 10 (2003) 265.
[59] A.P. Hitchcock, P. Hitchcock, C. Jacobsen, C. Zimba, B. Loo, E. Rotenberg, J. Denlinger and R. Kneedler, *aXis2000—program available from http://unicorn.mcmaster.ca/aXis2000.html* (1997).
[60] S.W. Gaarenstroom, J. Vac. Sci. Technol. A 15 (1997) 470.
[61] D. Li, G.M. Bancroft, M. Kasrai, M.E. Fleet, X.H. Feng and K.H. Tan, Am. Mineralogists 79 (1994) 785.
[62] D. Li, M.E. Fleet, G.M. Bancroft, M. Kasrai and Y. Pan, J. Non-Cryst. Solids 188 (1995) 181.
[63] J.M. Chen, J.K. Simons, K.H. Tan and R.A. Rosenberg, Phys. Rev. B. 48 (1993) 10047.
[64] Z. Yin, M. Kasrai, G.M. Bancroft, K.H. Tan and X. Feng, Phys. Rev. B. 51 (1995) 742.
[65] M.L. Suominen Fuller, M. Kasrai, G.M. Bancroft, K. Fyfe and K.H. Tan, Tribol. Int. 31 (1998) 627.
[66] R.C. Coy and R.B. Jones, ASLE Trans. 24 (1981) 77.
[67] J.J. Dickert and C.N. Rowe, J. Org. Chem. 32 (1967) 647.
[68] S.A. Syed Asif, K.J. Wahl, R.J. Colton and O.L. Warren, J. Appl. Phys. 90 (2001) 1192.
[69] J.B. Pethica and W.C. Oliver, Phys. Scr. T17 (1987) 61.
[70] S.A. Syed Asif, K.J. Wahl and R.J. Colton, Rev. Sci. Instr. 70 (1999) 2408.
[71] K.J. Wahl, S.A. Syed Asif and R.J. Colton, in: *Interfacial Properties on the Submicrometer Scale*, Vol. 781, eds. J. Frommer and R.M. Overney (American Chemical Society, Washington DC, 2001) 198.